P69 USING THE NASA-UNIFIED WRF TO ASSESS THE IMPACTS OF REAL-TIME VEGETATION ON SIMULATIONS OF SEVERE WEATHER

Jonathan L. Case[1]*, Frank J. LaFontaine[2], Sujay V. Kumar[3], and Christa D. Peters-Lidard[4]

[1]ENSCO, Inc./Short-term Prediction Research and Transition (SPoRT) Center, Huntsville, AL
[2]Raytheon/SPoRT Center, Huntsville, AL
[3]SAIC/NASA Goddard Space Flight Center, Greenbelt, MD
[4]NASA Goddard Space Flight Center, Greenbelt, MD

1. INTRODUCTION

Since June 2010, the NASA Short-term Prediction Research and Transition (SPoRT; Goodman et al. 2004; Darden et al. 2010; Stano et al. 2012; Fuell et al. 2012) Center has been generating a real-time Normalized Difference Vegetation Index (NDVI) and corresponding Green Vegetation Fraction (GVF) composite based on reflectances from NASA's Moderate Resolution Imaging Spectroradiometer (MODIS) instrument. This dataset is generated at 0.01° resolution across the Continental United States (CONUS), and updated daily. The goal of producing such a vegetation dataset is to improve over the default climatological GVF dataset in land surface and numerical weather prediction models, in order to have better simulations of heat and moisture exchange between the land surface and the planetary boundary layer. Details on the SPoRT/MODIS vegetation composite algorithm are presented in Case et al. (2011).

Vegetation indices such as GVF and Leaf Area Index (LAI) are used by land surface models (LSMs) to represent the horizontal and vertical density of plant vegetation (Gutman and Ignatov 1998), in order to calculate transpiration, interception and radiative shading. Both of these indices are related to the NDVI; however, there is an inherent ambiguity in determining GVF and LAI simultaneously from NDVI, as described in Gutman and Ignatov (1998). One practice is to specify the LAI while allowing the GVF to vary both spatially and temporally, as is done in the Noah LSM (Chen and Dudhia 2001; Ek et al. 2003). Operational versions of Noah within several of the National Centers for Environmental Prediction (NCEP) global and regional modeling systems hold the LAI fixed, while the GVF varies according to a global monthly climatology. This GVF climatology was derived from NDVI data on the NOAA Advanced Very High Resolution Radiometer (AVHRR) polar orbiting satellite, using information from 1985 to 1991 (Gutman and Ignatov 1998; Jiang et al. 2010). Representing data at the mid-point of every month, the climatological dataset is on a grid with 0.144° (~16 km) spatial resolution and is distributed with the community WRF model (Ek et al. 2003; Jiang et al. 2010; Skamarock et al. 2008).

A limitation of the climatological dataset is that the annual cycle of GVF is always represented the same in models from one year to the next. In reality, the response of vegetation to meteorological and climate conditions varies between seasons and years based on anomalous weather and climate features. For example, an unusual hard freeze or drought can lead to a vegetative response that is quite different than the climatological representation. In addition, the dated information (1985–1991) used to create the default GVF climatology, coupled with the relatively coarse spatial resolution, may not be representative of current vegetative conditions in today's high-resolution numerical models. Recent land use changes due to urban sprawl may also contribute to misrepresentations in the models.

Previous studies have examined near real-time vegetation datasets derived from the NOAA/AVHRR satellite (Jiang et al. 2010) and demonstrated its potential utility on real-time modeling (Crawford et al. 2001; Kurkowski et al. 2003; James et al. 2009). Other studies have examined vegetation datasets derived from the NASA MODIS instruments (Miller et al. 2006; Ruhge and Barlage 2011), but few have demonstrated a real-time MODIS vegetation dataset for regional, high-resolution modeling applications (e.g. Kain et al. 2010). This paper and companion poster examines the impacts of the real-time MODIS GVF dataset on model simulations of specific severe weather episodes from 2010 and 2011. This study employs the use of the NASA Land Information System (LIS) and its coupling to the Advanced Research WRF (ARW; Skamarock et al. 2008) model within the NASA-Unified WRF (NU-WRF) framework. The remainder of this paper is organized as follows. Section 2 gives background information on the NASA LIS and NU-WRF modeling frameworks. Section 3 presents the methodology used for the simulation experiments. Results are shown in Section 4 followed by a summary in Section 5.

2. LAND INFORMATION SYSTEM (LIS) AND NASA-UNIFIED WRF (NU-WRF)

The NASA LIS is a high performance land surface modeling and data assimilation system that integrates satellite-derived datasets, ground-based observations and model reanalyses to force a variety of LSMs (Kumar et al. 2006; Peters-Lidard et al. 2007). By using scalable, high-performance computing and data management technologies, LIS can run LSMs offline globally with a grid spacing as fine as 1 km to characterize land surface states and fluxes.

The LIS is a component of the NU-WRF system, which is a unification of several NASA modeling capabilities into a single package based on the ARW dynamical core. Features of the NU-WRF package include unique Goddard microphysics and

*Corresponding author address: Jonathan Case, ENSCO, Inc., 320 Sparkman Dr., Room 3062, Huntsville, AL, 35805. Email: Jonathan.Case-1@nasa.gov

short/longwave radiation physics options for the ARW (Chou and Suarez 1999, 2001), the Goddard Satellite Data Simulator Unit (Masunaga et al. 2010), the Goddard Chemistry Aerosol Radiation and Transport model (Chin et al. 2000ab, 2002, 2004; Ginoux et al. 2001), coupling between the LIS and ARW (Kumar et al. 2007) and companion land surface verification toolkit (Kumar et al. 2012), atmospheric verification with the NCAR Model Evaluation Tools, and numerous post-processing capabilities. This experiment takes advantage of the LIS/ARW coupling in NU-WRF to examine model sensitivity to the new MODIS GVF dataset.

3. SIMULATION EXPERIMENT DESIGN

For these set of experiments, we employed a convection-allowing model configuration mimicking the ARW as run in real-time at the National Severe Storms Laboratory (NSSL) to support the Storm Prediction Center (SPC) and various NWS forecast offices (Kain et al. 2010). The NSSL WRF model runs at 4-km horizontal grid spacing covering the CONUS and adjacent portions of northern Mexico, southern Canada, and Pacific/Atlantic Oceans. It is integrated daily for 36 hours from a 0000 UTC initialization time using NCEP NAM initial and boundary conditions. Refer to the following web site for real-time output: http://www.nssl.noaa.gov/wrf/.

The LIS and NU-WRF were both configured to use the International Geosphere-Biosphere Programme (IGBP) land-use classification (Loveland et al. 2000) as applied to the MODIS instrument (Friedl et al. 2010). All static and dynamic land surface fields were masked based on the IGBP/MODIS land-use classes. The soil properties were represented by the State Soil Geographic (STATSGO; Miller and White 1998) database. Additional parameters include an albedo climatology (Briegleb et al. 1986), a 0.05° resolution maximum snow surface albedo derived from MODIS (Barlage et al. 2005), and a deep soil temperature climatology (serving as a lower boundary condition for the soil layers) at 3 meters below ground, derived from 6 years of Global Data Assimilation System (GDAS) 3-hourly averaged 2-m air temperatures using the method described in Chen and Dudhia (2001).

To provide a proper land surface initialization, an "offline" LIS spin-up simulation was conducted with 4-km horizontal grid spacing over a CONUS domain identical to the NSSL WRF model configuration. In the offline spin-up run, the Noah LSM was integrated apart from a full NWP model within the LIS framework using global atmospheric analyses from the NCEP GDAS (Parrish and Derber 1992; Derber and Wu 1998; NCEP EMC 2004) to drive the integration of land surface variables. The offline LIS run was cold-started on 1 June 2008 with a uniform first-guess soil temperature and volumetric soil moisture of 290 K and 25%, respectively, in all soil layers. The Noah LSM was integrated for a time period of 2 years to 1 June 2010, using a time step of 30 minutes. A sufficiently long integration time, or "spin-up", is necessary to ensure that the model states reach a fine-scale equilibrium with the forcing meteorology acting on the high-resolution input fields (Cosgrove et al. 2003; Rodell et al. 2005). During the two-year spin-up integration, the AVHRR GVF monthly climatology was used. After 0000 UTC 1 June 2010, the spin-up run was re-started for two separate offline integrations, a control run that continued using the AVHRR GVF climatology, and an experimental run that employed the daily SPoRT/MODIS GVF during the period of study from 1 June 2010 through Spring 2011 (illustrated in Figure 1).

Two coupled LIS/ARW simulations within the NU-WRF framework were run out to 36 hours, initialized at 0000 UTC for each case day of interest. Each control coupled simulation was initialized with the AVHRR GVF climatology and land surface fields from the control offline LIS run. Meanwhile, the experimental coupled simulation was initialized with SPoRT/MODIS daily GVF and land surface data from the experimental offline LIS output that incorporated the MODIS GVF. Output of the two different coupled runs were then compared graphically to examine the impacts that the MODIS GVF had on the ARW simulations compared to the GVF climatology dataset.

The severe weather cases simulated include several events from the 2010 and 2011 Spring and Summer. The events simulated include:

- 10-11 June 2010: Colorado supercells,
- 15 June 2010: severe wind episode in the Southeastern U.S.,
- 17 June 2010: tornado outbreak in North Dakota and Minnesota,
- 17 July 2010: Upper Midwest tornadoes and severe wind event,
- 23 July 2010: Vivian, SD record hail event,
- 24-26 October 2010: multi-day severe event and major cyclone across the Southern U.S. and Mississippi Valley,
- 27 April 2011: southeastern U.S. super tornado outbreak,
- 22 May 2011: Joplin, MO EF-5 tornado day,
- 24-25 May, 2011: 2-day tornado and severe weather outbreak from the Southern Plains to the Mississippi Valley.

While the simulations were made for all these cases, only results selected cases are presented.

4. IMPACT RESULTS

A general observation on the real-time MODIS GVF impacts is that the differences in model simulations are relatively subtle in many cases examined. Several factors led to a limited impact of the real-time GVF data on the model forecasts:

- Limited surface heating due to prevailing cloud cover and pre-existing precipitation,
- Strong synoptic dynamics that overwhelm differential surface heating,
- Overall poor model performance due to atmospheric initial condition uncertainty and/or random model errors.

The ideal case is one that consists of a reasonably accurate control simulation along with limited cloud cover and precipitation prior to the severe weather event. Such a scenario maximizes the contributions of differential sensible and latent heat fluxes due to variations in GVF and minimizes the contaminating effects of pre-existing clouds and precipitation systems.

Several cases experienced limited impact due largely to the reasons listed above. Strong synoptic forcing and/or prevailing clouds/precipitation resulted in nominal impact of MODIS GVF on 17 June 2010, 24-26 October 2010, and 27 April 2011. A general poor model performance occurred on 10-11 June 2010 and 15 June 2010 (large location errors in convection and substantial false alarm regions). On 24 May 2011, both the control and experimental model runs missed the main convective initiation event across western and central Oklahoma.

Out of all the simulated events, two cases stood out as having the most positive impact with the inclusion of the real-time MODIS GVF: 17 July 2010 and 22 May 2011. These cases both exhibited substantial surface heating during the daytime, thereby maximizing the differences in surface fluxes and evapotranspiration, leading to changes in the evolution of simulated convection. A summary of the SPC severe reports for both these days is given in Figure 2. On 17 July 2010, numerous tornado, large hail, and severe wind reports occurred over eastern South Dakota, central Minnesota, and Iowa, which is the focus area subset for presenting model comparisons. On 22 May 2011, numerous tornadoes and hail/wind severe reports occurred from northeastern Oklahoma to northern Wisconsin; however, model sensitivity results are focused on a geographical subset centered on Joplin, MO.

4.1 17 July 2010 case

In the Upper Midwest focus area, the pattern of GVF were broadly similar, but with notable differences. The High Plains from Nebraska to North Dakota generally had higher MODIS GVF up to 20% or more, while lower MODIS GVF occurred across western Illinois and northern Minnesota (Figure 3). A relative minimum in GVF over urban regions shows up more distinctly in the MODIS daily product.

This day featured an optimal scenario for examining the sensitivity of the model to the new GVF dataset in that surface heating was minimally impacted by prevailing modeled cloud cover, as seen in the 19-h forecast total column condensate (sum of vertically-integrated cloud and precipitation microphysics) of Figure 4. Both the control and sportgvf runs produced very little cloudiness during the several hours of peak solar heating. Consequently, the differences in GVF translated almost directly into a change in the partitioning of the incoming shortwave radiation into sensible and latent heat fluxes. Regions of higher MODIS GVF from Nebraska to North Dakota (Figure 3) simultaneously led to a reduction in the sensible heat flux by 50+ W m^{-2} and an increase in latent heat flux up to 100+ W m^{-2} in the 19-h WRF forecast (Figure 5).

These modifications in the heat fluxes due to GVF translated into changes in the 21-h forecast 2-m temperature and dew point, as seen in Figure 6 and Figure 7, respectively. The western part of the focus area that had higher MODIS GVF (Figure 3) experienced a net decrease (increase) in the 2-m temperature (dew point), typically on the order of 1–2°, although local increases in dew point exceeded 4°C at 21 hours. The slightly lower 2-m temperatures in the sportgvf run over South Dakota are more in-line with the observations plotted in Figure 6; however, both model runs generally under-estimated the 2-m temperatures over eastern Nebraska, and southern and western Iowa. Conversely, portions of northern Minnesota and western Illinois have the opposite response where the GVF was lower in the sportgvf run.

Objective verification statistics of the 2-m temperature and 2-m dew point clearly illustrate the differences due to the new GVF dataset. The mean error or bias in the 2-m temperature shows systematically cooler simulated temperatures up to -1.5°C over the Northern Plains NCEP verification region (NPL, upper-left panel of Figure 8), which experienced the largest increases in GVF over the control/AVHRR climatology. Similarly, the NPL verification region also had systematically higher 2-m dew points up to ~2°C, especially beginning with the onset of the diurnal heating cycle after the 12-h forecast (upper-right panel of Figure 8). Further east over the Midwest verification region, very little systematic change is seen in the simulated 2-m temperature and dew point.

The net effect in the 21-h forecast (just prior to convective initiation) is an overall increase in the convective available potential energy (CAPE, Figure 9), especially over the western part of the focus area. Portions of eastern Nebraska to southeastern North Dakota had CAPE increases over 1000 J kg^{-1}. In this instance, the higher GVFs over the warm sector led to a greater influx of moisture into a shallower boundary layer (not shown), resulting in a net increase in moist static energy per unit mass within the boundary layer, despite small decreases in the 2-m temperature.

The impact of these GVF sensitivities to the model simulated precipitation was fairly subtle initially. Convective precipitation developed at 21 hours in both simulations over extreme southeastern North Dakota (not shown) and evolved into a bow-shaped line in southern Minnesota by 27 hours (Figure 10). The difference in the 1-h simulation precipitation at 27 hours (lower left of Figure 10) suggests that the sportgvf run was a bit slower and more intense than the control over southern Minnesota. Both simulations incorrectly produced a nearly continuous line of precipitation while the observed precipitation resembled a more discrete mode (lower-right panel). However, over the next several hours, the control simulation quickly moved the precipitation into northern Missouri, while the sportgvf run regenerated/back-built convection more similar to the observed evolution. By 33-h (0900 UTC 18 July), the location and intensity of the sportgvf 1-h accumulated precipitation was more closely aligned with the Stage IV precipitation analysis compared to the control run (Figure 11). Objective verification statistics support these subjective interpretations, as indicated by the higher values of Critical Success Index scores in the sportgvf run, especially associated with the nocturnal precipitation after ~31 hours (Figure 12). This improved simulated precipitation during this time is likely due to the higher residual CAPE in the sportgvf run over eastern Nebraska and western Iowa during these forecast hours (not shown).

4.2 22 May 2011 case

The climatology and MODIS GVF on 22 May 2011 have similar broad-scale patterns in the focus region, with maximum GVF over the forests of eastern Oklahoma, northwestern Arkansas, and southern Missouri, and minimum GVF in the agricultural belt of the Mississippi River Valley (Figure 13). The largest differences between the control GVF and real-time MODIS GVF are the enhanced gradient in southeast Missouri, lower MODIS GVF in southern Arkansas, and a band of slightly higher MODIS GVF from northeast Texas to central Missouri (bottom of Figure 13).

The 22 May 2011 event was not quite as clean as 17 July 2010, as cloud cover and ongoing precipitation occurred across part of the interest area. A reduction in cloud cover occurred in the sportgvf model run over Arkansas (not shown), likely due to the lower GVF in the sportgvf model run, which provided a reduced rate of evapotranspiration into the boundary layer. At the 21-h forecast just prior to initiation of the convection that affected Joplin, MO, the simulated CAPE fields depicted very high instability of 3000–4000+ J kg^{-1} from southeast Oklahoma to southwest Missouri (Figure 14). The sportgvf run generally simulated slightly higher CAPE across much of Missouri, whereas the largest CAPE differences occurred over eastern Arkansas where the control run initially produced more convection than the sportgvf run (not shown).

Two hours later at 2300 UTC, both model simulations had a cluster of convective precipitation over southeast Kansas into southwest Missouri (top panels of Figure 15), corresponding quite well to the observed position of convection that eventually produced the EF-5 tornado in Joplin, MO. However, precipitation rates were more intense in the sportgvf run at over 25 mm h^{-1}, more closely aligned with the Stage IV precipitation analysis (bottom-right of Figure 15). Following the Joplin, MO tornado, the convective precipitation evolved into a bow-shaped squall line in northern Arkansas and southern Missouri by 0300 UTC (Figure 16). The control run moved the convection more quickly into Arkansas and did not simulate the bowed structure of the line as well as the sportgvf run. The sportgvf run also back-built the convection into far northeast Oklahoma, more similar to the Stage IV precipitation analysis (bottom right of Figure 16). In addition, the sportgvf run reduced the false alarm precipitation region over central Arkansas at this time.

These two cases experienced some improvements in the simulated precipitation systems as a result of incorporating real-time MODIS GVF in place of the monthly AVHRR GVF climatology. These results are not typical of the numerous other events simulated. Nevertheless, the favorable impacts indicate the potential for model improvements in some warm-season severe convective events.

5. SUMMARY

This paper presented a technique for assessing the impact of real-time MODIS GVF data on numerical forecasts of various severe weather episodes from 2010 and 2011. The NU-WRF modeling system was the tool of choice to incorporate the MODIS GVF into both the Land Information System and ARW model. The coupling between LIS and the ARW model within NU-WRF enabled a uniquely configured set of static and time-varying land surface model parameters to run identically in both the LIS offline spin-up run and the ARW model. WRF simulations were initialized with the LIS offline output for any given event, and forecasts were made on a Continental U.S. domain with 4-km grid spacing, using an identical configuration as in the real-time WRF runs at NSSL.

Most severe weather events simulated did not see appreciable impacts or improvements by incorporating real-time MODIS GVF, often due to a poor control simulation, strong synoptic forcing that overwhelms land-atmosphere interactions, or pre-existing clouds and precipitation. However, the two cases highlighted in this paper saw differential sensible and latent heat fluxes caused by the GVF differences, which led to notable improvements in the simulated convective precipitation. The documented improvements in these events indicate the potential utility in using real-time, high-resolution vegetation information in convection-allowing model simulations under certain regimes.

6. ACKNOWLEDGEMENTS/DISCLAIMER

This research was funded by Dr. Tsengdar Lee of the NASA Science Mission Directorate's Earth Science Division in support of the SPoRT program at the NASA MSFC, as well as funding provided by the NASA Modeling Analysis and Prediction Solicitation NNH08ZDA001N-MAP (PI: Peters-Lidard/GSFC). Computational resources for this work were provided by the NASA Center for Climate Simulation at the NASA Goddard Space Flight Center. Mention of a copyrighted, trademarked or proprietary product, service, or document does not constitute endorsement thereof by the authors, ENSCO Inc., the University of Missouri, Raytheon, the SPoRT Center, the National Aeronautics and Space Administration, or the United States Government. Any such mention is solely for the purpose of fully informing the reader of the resources used to conduct the work reported herein.

7. REFERENCES

Barlage, M., X. Zeng, H. Wei, and K. E. Mitchell, 2005: A global 0.05° maximum albedo dataset of snow-covered land based on MODIS observations. *Geophys. Res. Lett.,* **32,** L17405, doi:10.1029/2005GL022881.

Briegleb, B. P., P. Minnis, V. Ramanathan, and E. Harrison, 1986: Comparison of regional clear-sky albedos inferred from satellite observations and model computations. *J. Climate Appl. Meteor.,* **25,** 214-226.

Case, J. L., F. J. LaFontaine, S. V. Kumar, and G. J. Jedlovec, 2011: A real-time MODIS vegetation composite for land surface models and short-term forecasting. Preprints, *15th Symp. on Integrated Observing and Assimilation Systems for the Atmosphere, Oceans, and Land Surface,* Seattle, WA, Amer. Meteor. Soc., 11.2. [Available online at http://ams.confex.com/ams/91Annual/webprogram/Manuscript/Paper180639/Case_etal_2011AMS-15IOAS-AOLS_11.2_FINAL.pdf]

Chen, F., and J. Dudhia, 2001: Coupling an advanced land-surface/hydrology model with the Penn State/NCAR MM5 modeling system. Part I: Model description and implementation. *Mon. Wea. Rev.,* **129,** 569-585.

Chin, M., R. B. Rood, S.-J. Lin, J.-F. Müller, and A. M. Thompson, 2000a: Atmospheric sulfur cycle simulated in the global model GOCART: Model description and global properties, *J. Geophys. Res.,* **105,** 24671-24687.

Chin, M., D. L. Savoie, B. J. Huebert, A. R. Bandy, D. C. Thornton, T. S. Bates, P. K. Quinn, E. S. Saltzman, and W. J. De Bruyn, 2000b Atmospheric sulfur cycle simulated in the global model GOCART: Comparison with field observations and regional budgets. *J. Geophys. Res.,* **105,** 24689-24712.

Chin, M., P. Ginoux, S. Kinne, O. Torres, B. N. Holben, B. N. Duncan, R. V. Martin, J. A. Logan, A. Higurashi, and T. Nakajima, T., 2002: Tropospheric aerosol optical thickness from the GOCART model and comparisons with satellite and sun photometer measurements. *J. Atmos., Sci.,* **59,** 461-483.

Chin, M., D. A. Chu, R. Levy, L. A. Remer, Y. J. Kaufman, B. N. Holben, T. Eck, T., and P. Ginoux, 2004: Aerosol distribution in the northern hemisphere during ACE-Asia: Results from global model, satellite observations, and sunphotometer measurements. *J. Geophy. Res.,* **109,** D23S90, doi:10.1029/2004JD004829.

Chou, M.-D., and M. J. Suzrez, 1999: A solar radiation parameterization for atmospheric studies. NASA Tech. Pre. NASA/TM-1999-10460, **vol. 15,** 38 pp.

Chou, M.-D., and M. J. Suzrez, 2001: A thermal infrared radiation parameterization for atmospheric studies. NASA/TM-2001-10406, **vol. 19,** 55 pp.

Cosgrove, B. A., and Coauthors, 2003: Real-time and retrospective forcing in the North American Land Data Assimilation System (NLDAS) project. *J. Geophys. Res.,* **108(D22),** 8842, doi:10.1029/2002JD003118, 2003.

Crawford, T. M., D. J. Stensrud, F. Mora, J. W. Merchant, and P. J. Wetzel, 2001: Value of incorporating satellite-derived land cover data in MM5/PLACE for simulating surface temperatures. *J. Hydrometeor.,* **2,** 453-468.

Darden, C. B., D. J. Nadler, B. C. Carcione, R. J. Blakeslee, G. T. Stano, and D. E. Buechler, 2010: Utilizing total lightning information to diagnose convective trends. *Bull. Amer. Meteor. Soc.,* **91,** 167-175.

Derber, J. C., and W.-S. Wu, 1998: The use of TOVS cloud-cleared radiances in the NCEP SST Analysis System. *Mon. Wea. Rev.,* **126,** 2287-2299.

Ek, M. B., K. E. Mitchell, Y. Lin, E. Rogers, P. Grunmann, V. Koren, G. Gayno, and J. D. Tarpley, 2003: Implementation of Noah land surface model advances in the National Centers for Environmental Prediction operational mesoscale Eta model. *J. Geophys. Res.,* **108 (D22),** 8851, doi:10.1029/2002JD003296.

Friedl, M. A., D. Sulla-Menashe, B. Tan, A. Schneider, N. Ramankutty, A. Sibley, and X. Huang, 2010: MODIS Collection 5 global land cover: Algorithm refinements and characterization of new datasets. *Remote Sens. Environ.,* **114,** 168-182.

Fuell, K. K., M. Smith, and G. J. Jedlovec, 2012: Early transition and use of NPP/VIIRS and GOES-R ABI and GLM products by NWS forecast offices. Preprints, *Eighth Annual Symposium on Future Operational Environmental Satellite Systems,* New Orleans, LA, Amer. Meteor. Soc., 5.4. [Available online at https://ams.confex.com/ams/92Annual/webprogram/Paper203161.html]

Ginoux, P., Chin, M., Tegen, I., Prospero, J., Holben, B., Dubovik, O., and Lin, S.-J., 2001: Sources and distributions of dust aerosols simulated with the GOCART model. *J. Geophys. Res.*, **106,** 20225-20273.

Gutman, G. and A. Ignatov, 1998: Derivation of green vegetation fraction from NOAA/AVHRR for use in numerical weather prediction models. *Int. J. Remote Sensing,* **19,** 1533-1543.

James, K. A., D. J. Stensrud, and N. Yussouf, 2009: Value of real-time vegetation fraction to forecasts of severe convection in high-resolution models. *Wea. Forecasting,* **24,** 187-210.

Jiang, L., and Coauthors, 2010: Real-time weekly global green vegetation fraction derived from advanced very high resolution radiometer-based NOAA operational global vegetation index (GVI) system. *J. Geophys. Res.,* **115,** D11114, doi:10.1029/2009JD013204.

Kain, J. S., S. R. Dembek, S. J. Weiss, J. L. Case, J. J. Levitt, and R. A. Sobash, 2010: Extracting unique information from high-resolution forecast models: Monitoring selected fields and phenomena every time step. *Wea. Forecasting,* **25,** 1536-1542.

Kumar, S. V., and Coauthors, 2006. Land Information System – An Interoperable Framework for High Resolution Land Surface Modeling. *Environmental Modeling & Software,* **21 (10),** 1402-1415, doi:10.1016/j.envsoft.2005.07.004.

Kumar, S. V., C. D. Peters-Lidard, J. L. Eastman, and W.-K. Tao, 2007: An integrated high-resolution hydrometeorological modeling testbed using LIS and WRF. *Environmental Modeling & Software,* **23 (2),** 169-181, doi: 10.1016/j.envsoft.2007.05.012.

Kumar, S. V., C. D. Peters-Lidard, J. Santanello, K. Harrison, Y. Liu, and M. Shaw, 2012: Land surface Verification Toolkit (LVT) – a generalized framework for land surface model evaluation. *Geosci. Model Dev. Discuss.,* **5,** 229-276, doi:10.5194/gmdd-5-229-2012.

Kurkowski, N. P., D. J. Stensrud, and M. E. Baldwin, 2003: Assessment of implementing satellite-derived land cover data in the Eta model. *Wea. Forecasting,* **18,** 404-416.

Loveland, T. R., B. C. Reed, J. F. Brown, D. O. Ohlen, Z. Zhu, L. Yang, and J. W. Merchant, 2000: Development of a global land cover characteristics database and IGBP DISCover from 1 km ABHRR data. *Int. J. Remote Sensing,* **21,** 1303-1330.

Masunaga, H., and Coauthors, 2010: Satellite Data Simulator Unit: A multisensory, multispectral satellite simulator package. *Bull Amer. Meteor. Soc.,* **91,** 1625-1632.

Miller, D. A. and R. A. White, 1998: A Conterminous United States multi-layer soil characteristics data set for regional climate and hydrology modeling. *Earth Interactions*, 2. [Available on-line at http://EarthInteractions.org]

Miller, J. M. Barlage, X. Zeng, H. Wei, K. Mitchell, and D. Tarpley, 2006: Sensitivity of the NCEP/Noah land surface model to the MODIS green vegetation fraction data set. *Geophys. Res. Lett.,* **33,** L13404, doi:10.1029/2006GL026636.

NCEP Environmental Modeling Center, 2004: SSI Analysis System 2004. NOAA/NCEP/Environmental Modeling Center Office Note 443, 11 pp., April, 2004. [Available online at http://www.emc.ncep.noaa.gov/officenotes/newernotes/on443.pdf]

Parrish, D. F., and J. C. Derber, 1992: The National Meteorological Center's spectral statistical-interpolation analysis system. *Mon. Wea. Rev.,* **120,** 1747-1763.

Peters-Lidard, C. D., and Coauthors, 2007: High-performance Earth system modeling with NASA/GSFC's Land Information System. *Innovations Syst. Softw. Eng.,* **3,** 157-165.

Ruhge, R. L., and M. Barlage, 2011: Integrating a real-time green vegetation fraction (GVF) product into the Land Information System (LIS). Preprints, *15th Symp. on Integrated Observing and Assimilation Systems for the Atmosphere, Oceans, and Land Surface,* Seattle, WA, Amer. Meteor. Soc., J14.4. [Available online at http://ams.confex.com/ams/91Annual/webprogram/Manuscript/Paper182739/amspaper.pdf]

Skamarock, W. C., J. B. Klemp, J. Dudhia, D. O. Gill, D. M. Barker, M. G. Duda, X-Y. Huang, W. Wang and J. G. Powers, 2008: A Description of the Advanced Research WRF Version 3, NCAR Technical Note, NCAR/TN–475+STR, 123 pp. [Available on-line at http://www.mmm.ucar.edu/wrf/users/docs/arw_v3.pdf]

Stano, G. T., 2012: Evaluation of NASA SPoRT's Pseudo-Geostationary Lightning Mapper Products in the 2011 Spring Program. Preprints, *Eighth Annual Symposium on Future Operational Environmental Satellite Systems,* New Orleans, LA, Amer. Meteor. Soc., P501. [Available online at https://ams.confex.com/ams/92Annual/webprogram/Manuscript/Paper203352/Stano_etal_2012AMS_501.pdf]

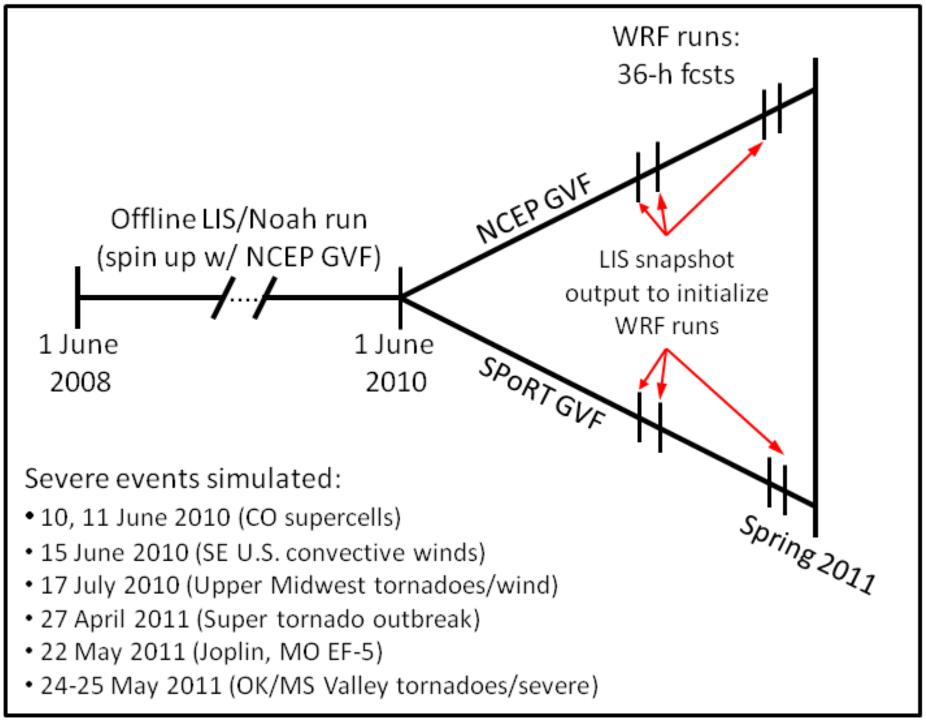

Figure 1. Methodology for spinning up the land surface fields within the LIS/Noah offline run, followed by the split into control (top line) and experimental (bottom line) LIS offline runs. Severe weather case dates listed were initialized using LIS land surface fields and the accompanying NCEP (AVHRR) or MODIS GVF.

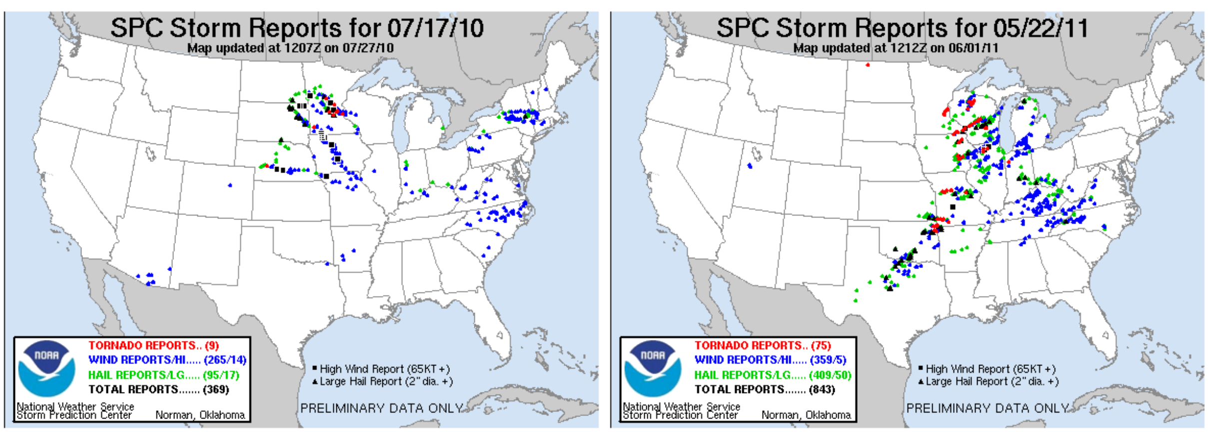

Figure 2. Storm Prediction Center (SPC) storm reports from 17 July 2010 (left), and 22 May 2011 (right).

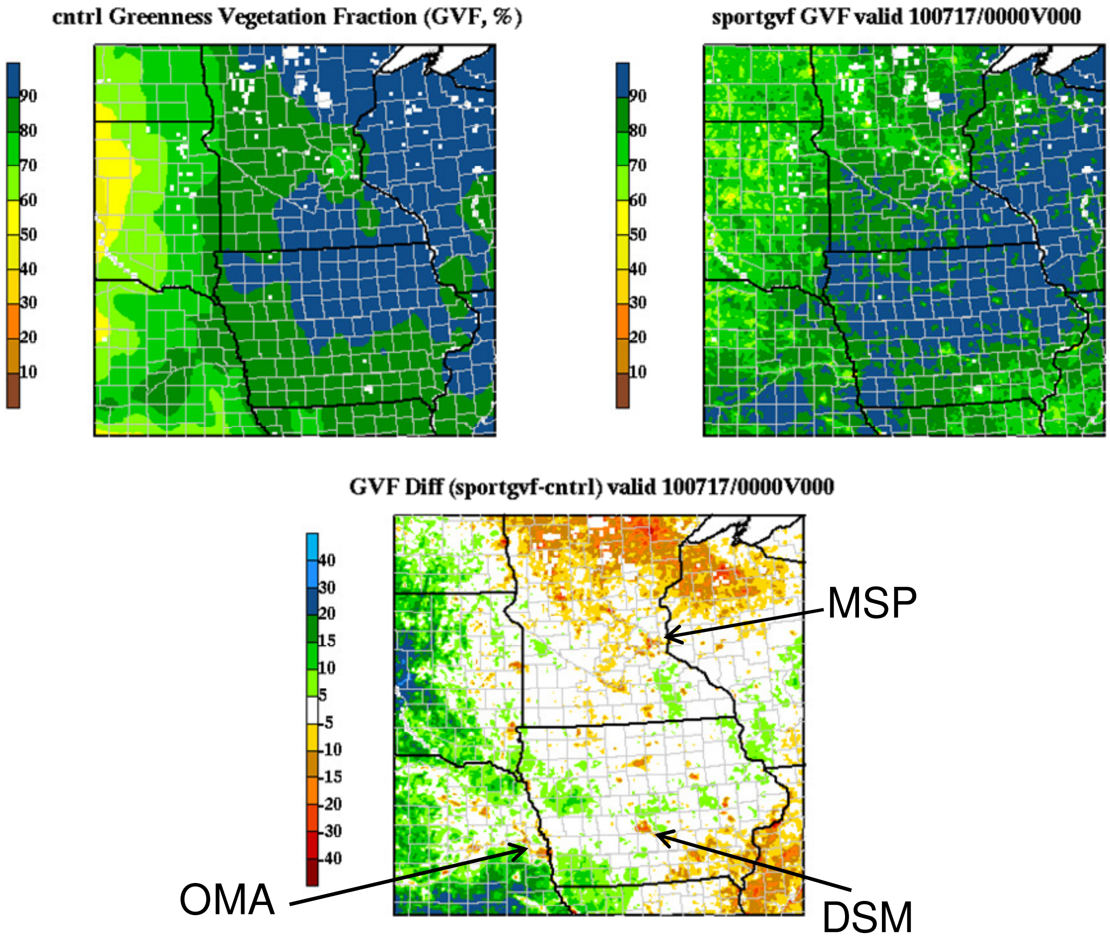

Figure 3. Comparison of the green vegetation fraction (GVF) in the 17 July 2010 simulations, depicting NCEP climatology GVF in the control simulation (upper-left), SPoRT/MODIS GVF in the experimental simulation (upper-right), and difference in GVF (SPoRT – NCEP, bottom panel).

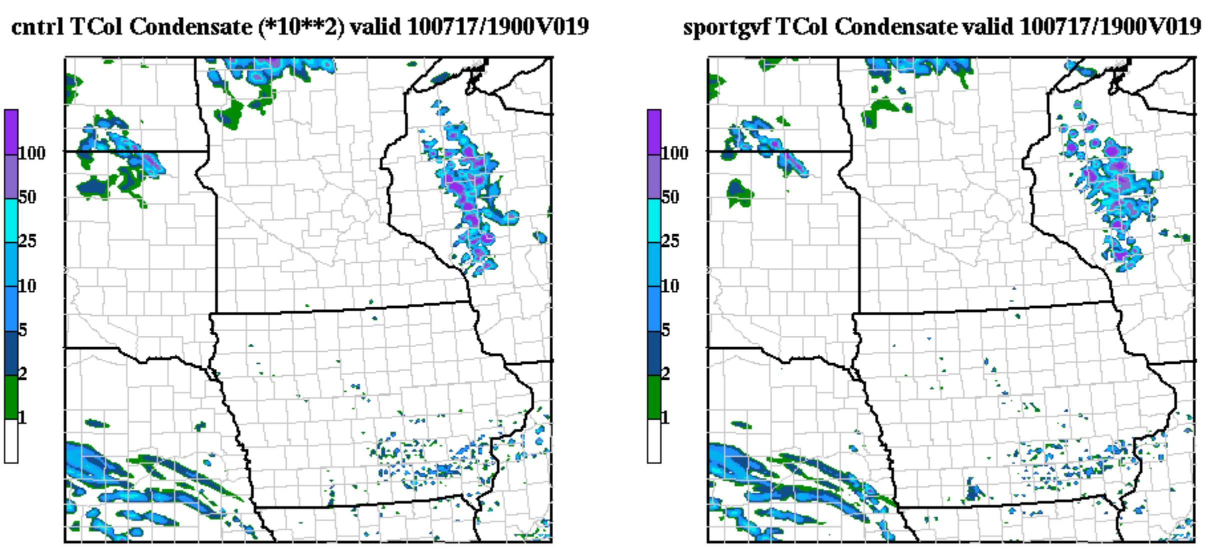

Figure 4. Total column cloud and precipitation condensate (g kg^{-1}) for the 19-h forecast valid 1900 UTC 17 July 2010 for the control run (left) and sportgvf experimental run (right).

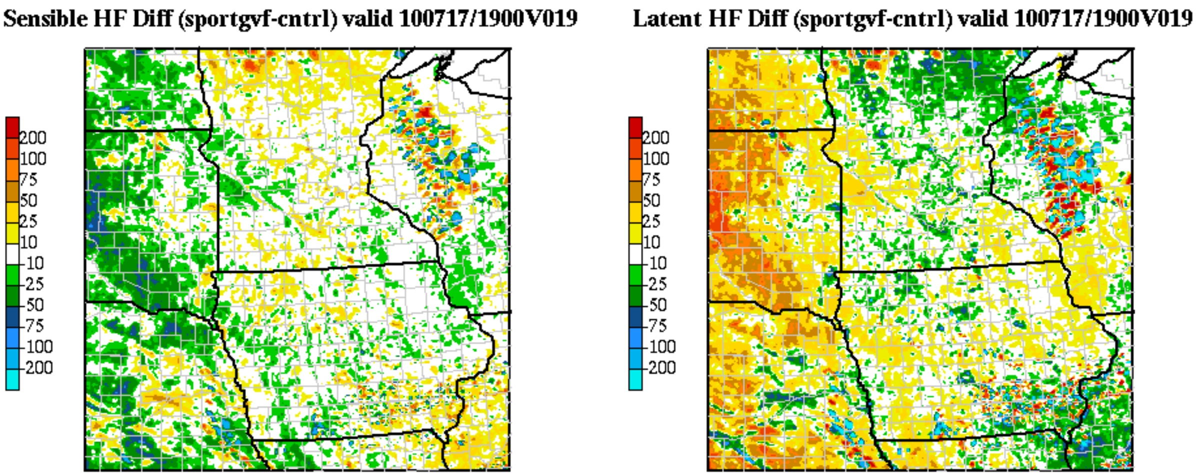

Figure 5. Difference in sensible (left) and latent heat flux (right, sportgvf – control in W m^{-2}) for the 19-h forecast valid 1900 UTC 17 July 2010.

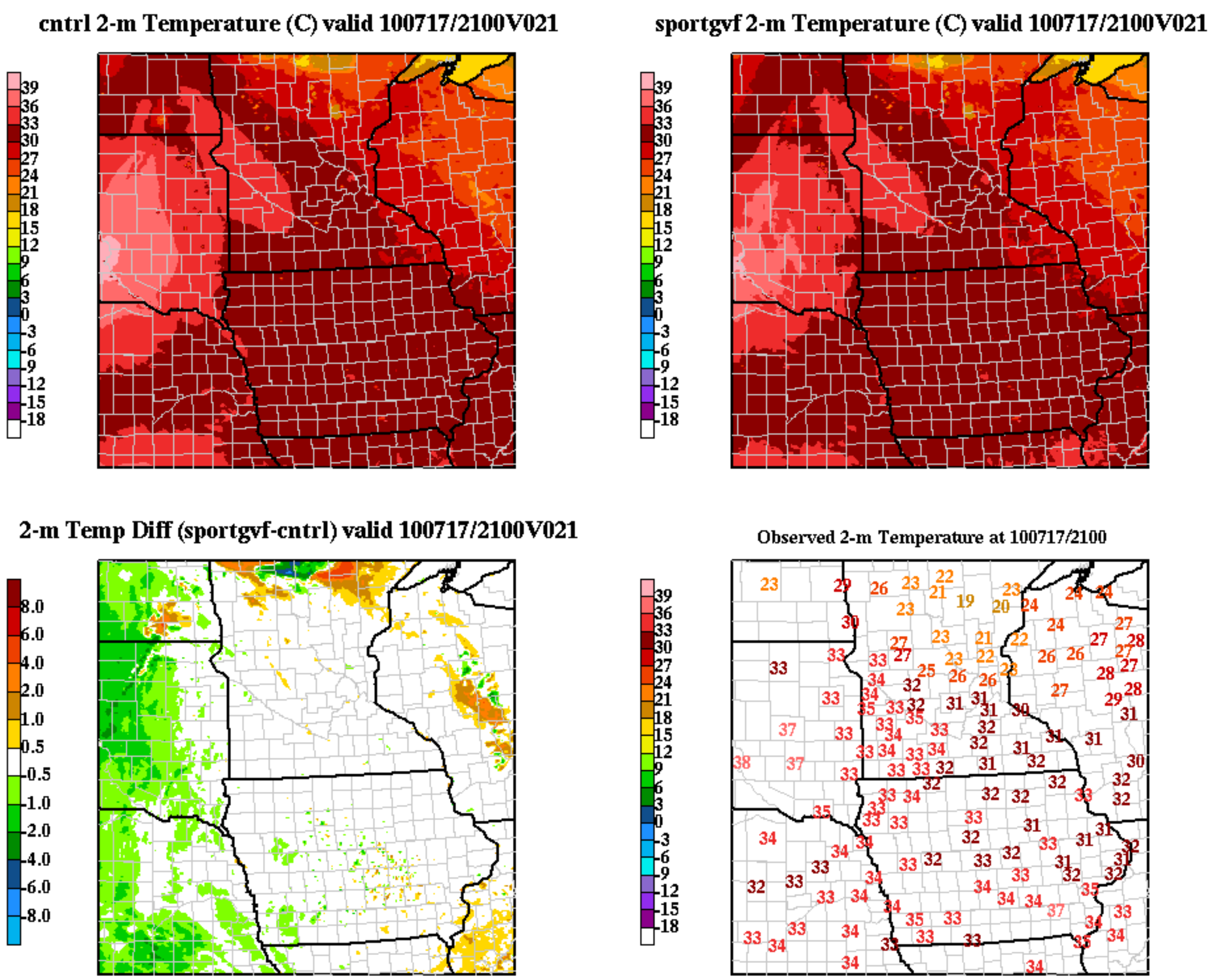

Figure 6. NU-WRF 21-h forecast 2-m temperature in °C for the control run (upper-left), sportgvf run (upper-right), difference (lower-left, sportgvf – control), and observed 2-m temperature (lower-right), valid 2100 UTC 17 July 2010, just prior to convective initiation.

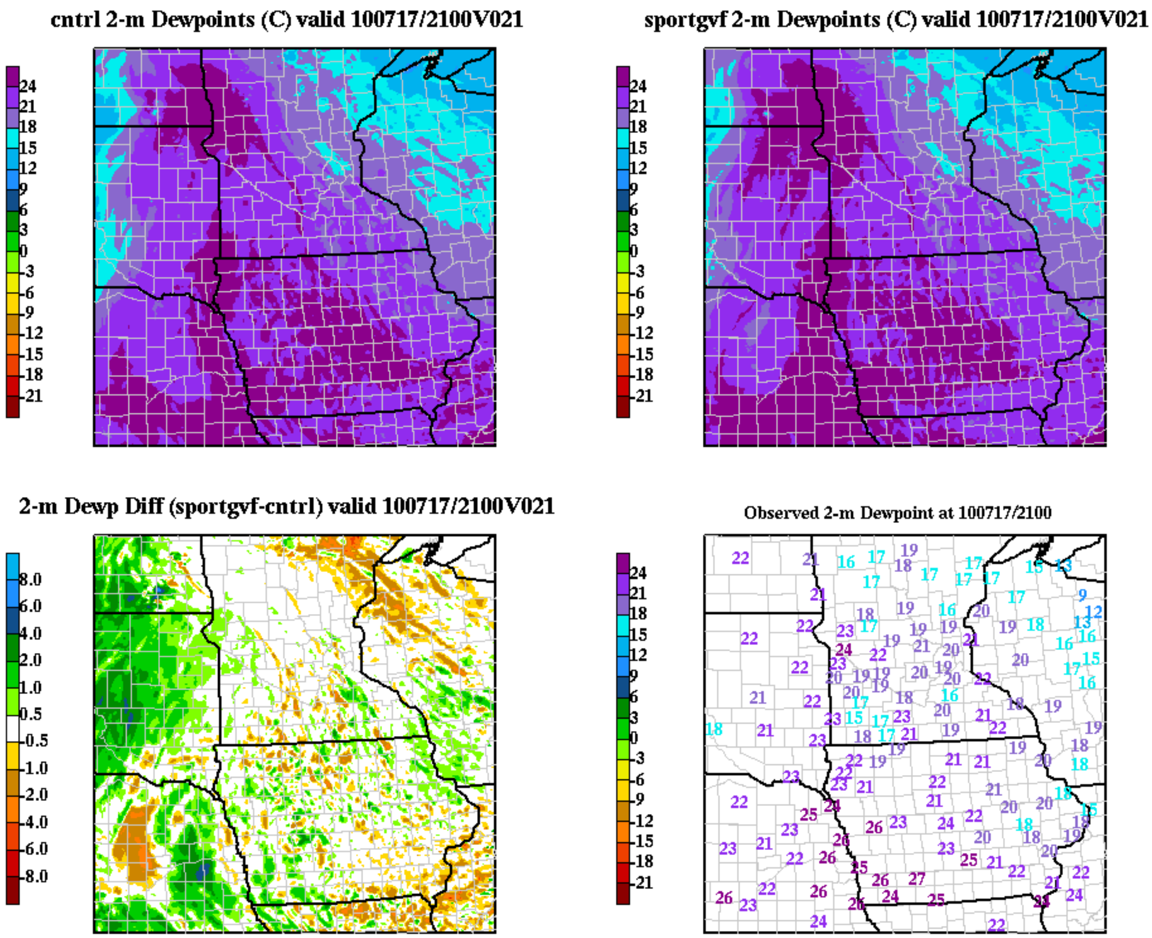

Figure 7. Same as in Figure 6, except for the 2-m dew point temperature.

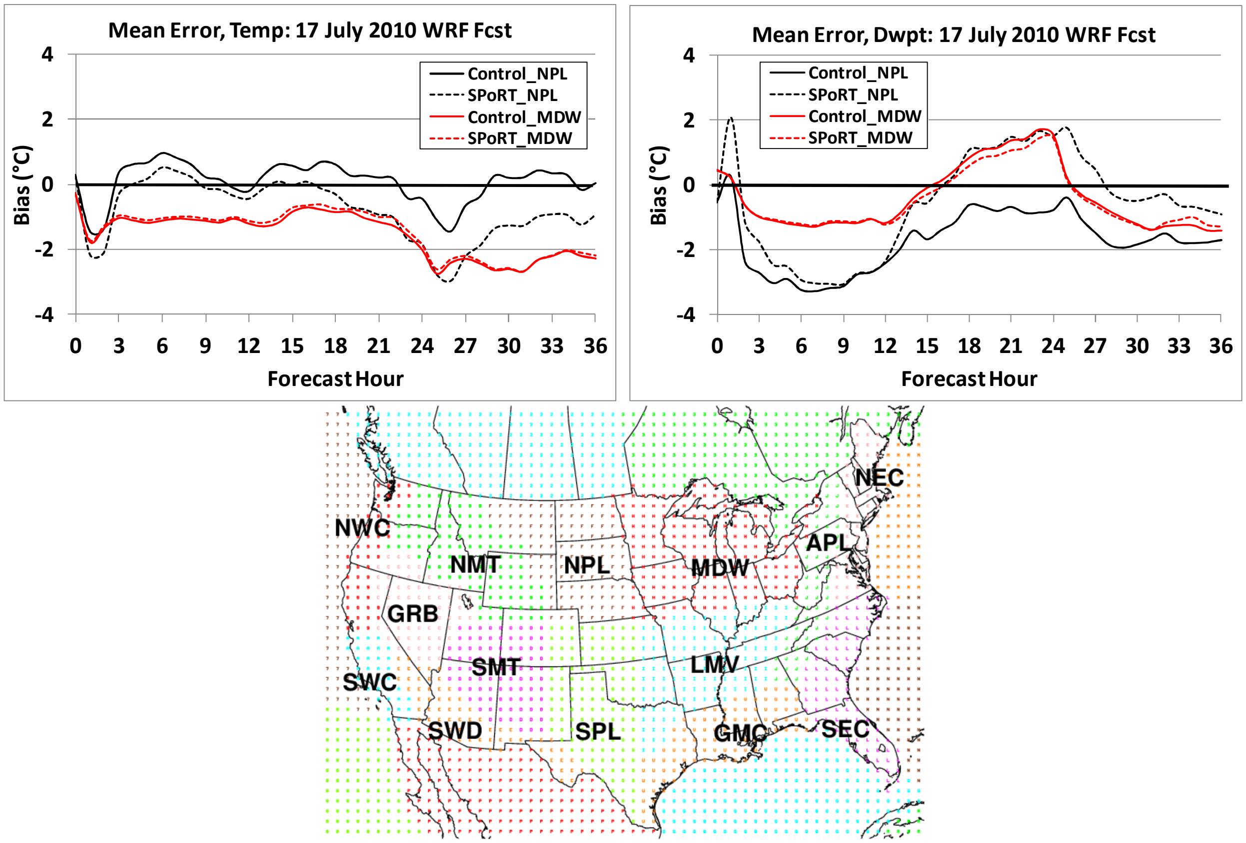

Figure 8. Mean error (bias) for 2-m temperature (upper-left) and 2-m dew point (upper-right) over the Northern Plains (NPL) and Midwest (MDW) NCEP verification regions as a function of forecast hour for the 17 July 2010 Control and SPoRT GVF model runs. NCEP verification regions are given in the bottom panel.

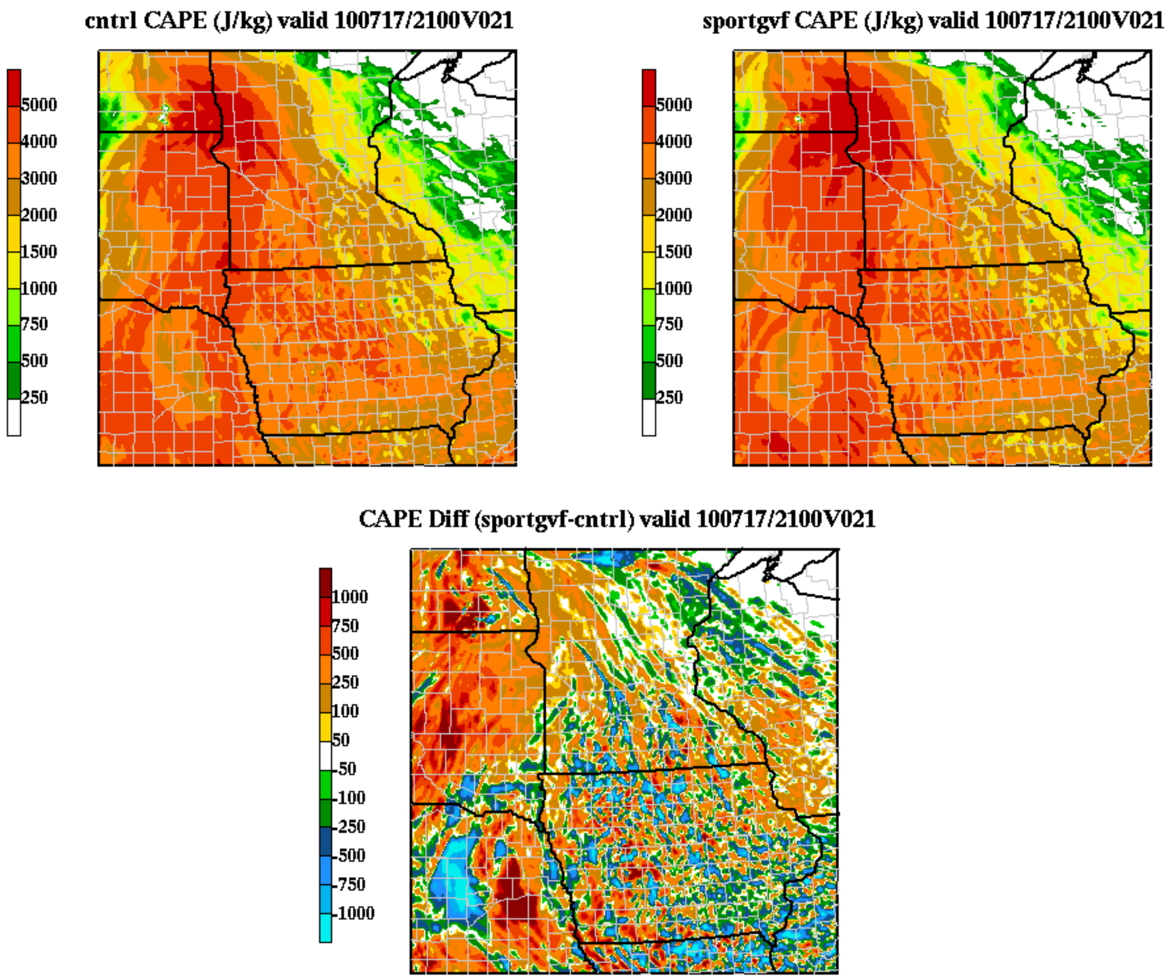

Figure 9. NU-WRF 21-h forecast convective available potential energy (CAPE, J kg^{-1}) for the control run (upper-left), sportgvf run (upper-right), and difference (bottom, sportgvf – control), valid 2100 UTC 17 July 2010, just prior to convective initiation.

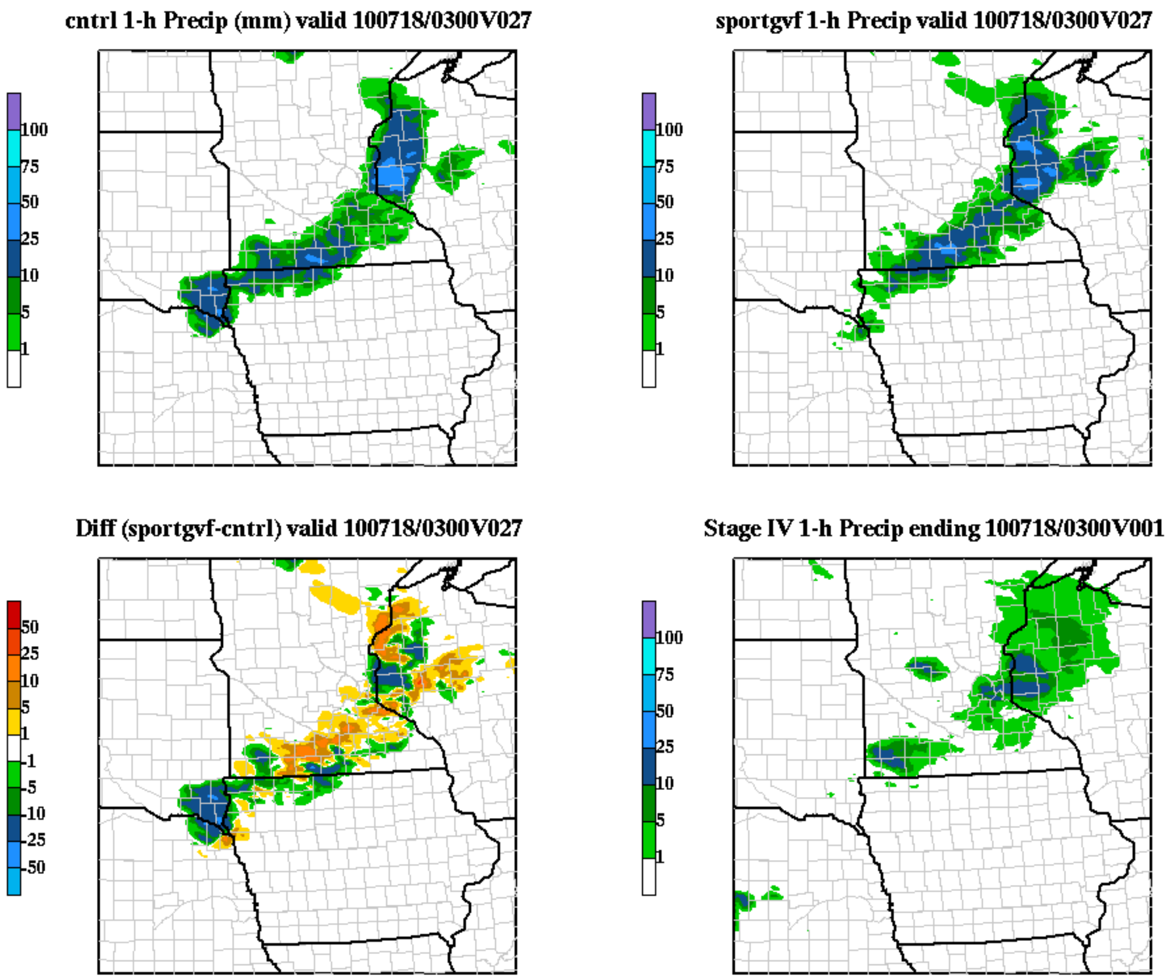

Figure 10. NU-WRF 1-h accumulated precipitation (mm) for the 27-h forecast of the control run (upper-left), sportgvf run (upper-right), difference (bottom-left, sportgvf – control), and stage IV precipitation analysis, valid for the hour ending 0300 UTC 18 July 2010.

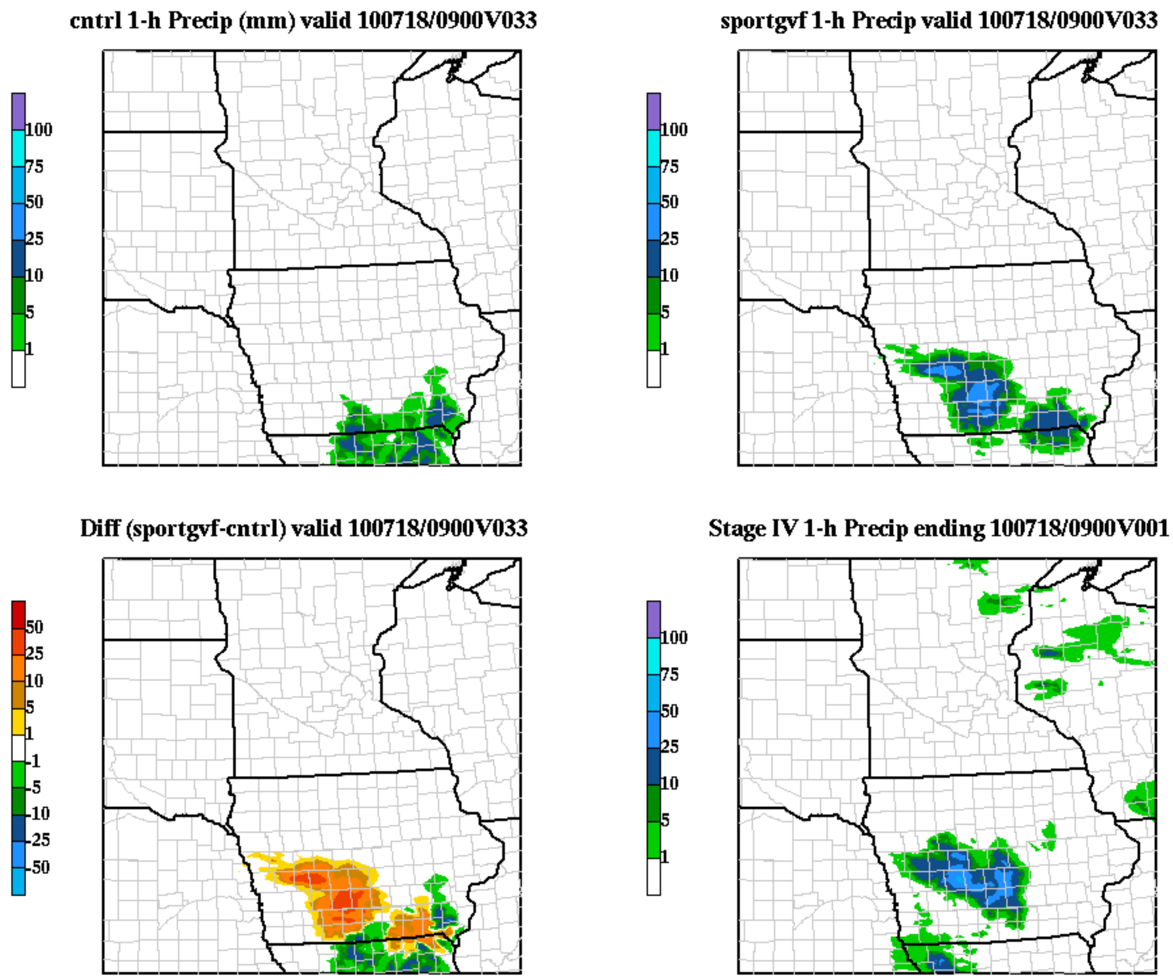

Figure 11. Same as in Figure 10, except for the 33-h forecast for the hour ending 0900 UTC 18 July 2010.

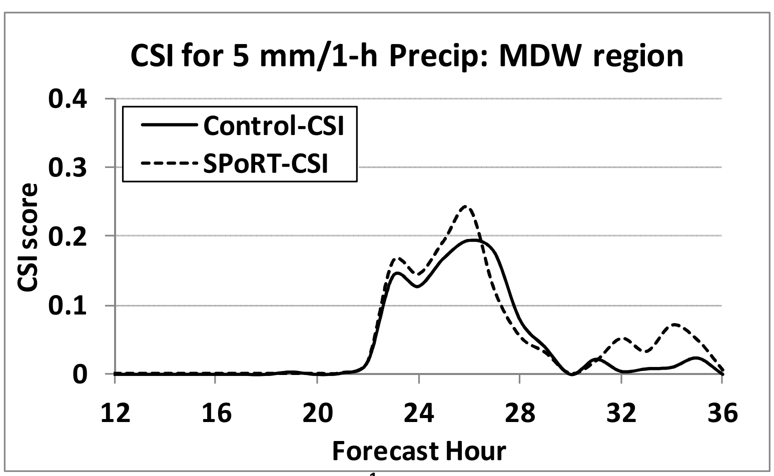

Figure 12. Critical Success Index (CSI) of the 5 mm (h^{-1}) accumulated precipitation for the 17 July 2010 Control and SPoRT GVF model runs between forecast hours 12 and 36 over the Midwest (MDW) NCEP verification region (MDW region shown in bottom panel of Figure 8).

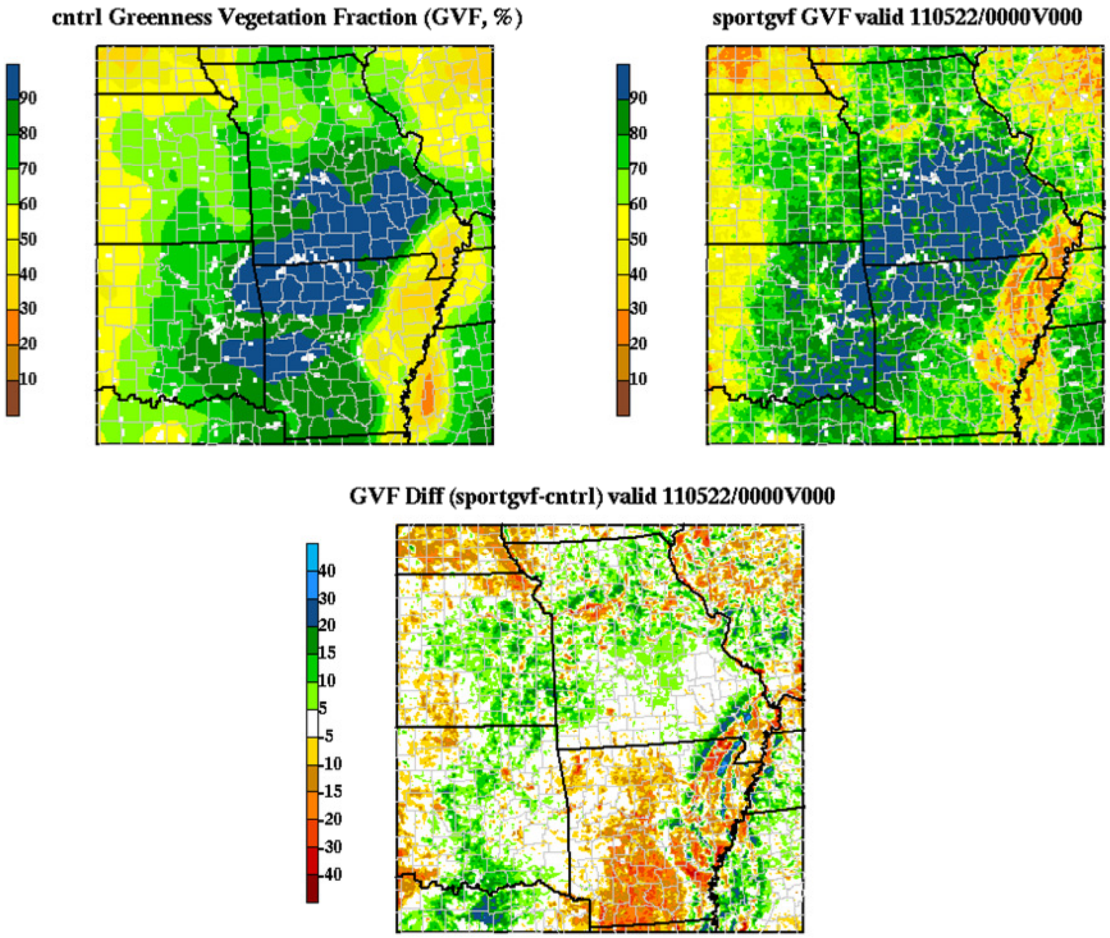

Figure 13. Same as in Figure 3, except for the 22 May 2011 simulations.

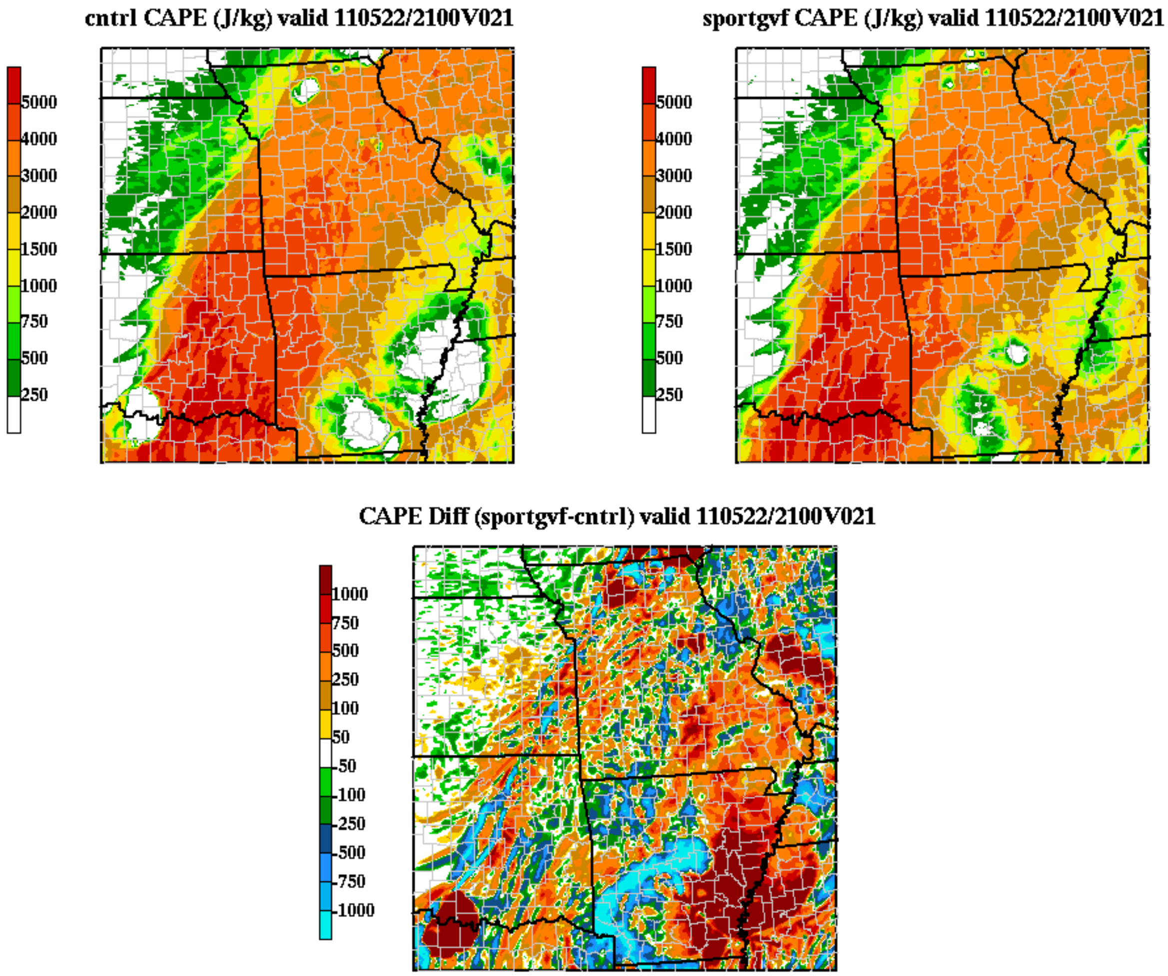

Figure 14. NU-WRF 21-h forecast CAPE (J kg^{-1}) for the control run (upper-left), sportgvf run (upper-right), and difference (bottom, sportgvf – control), valid 2100 UTC 22 May 2011, just prior to the initiation of convection that impacted Joplin, MO.

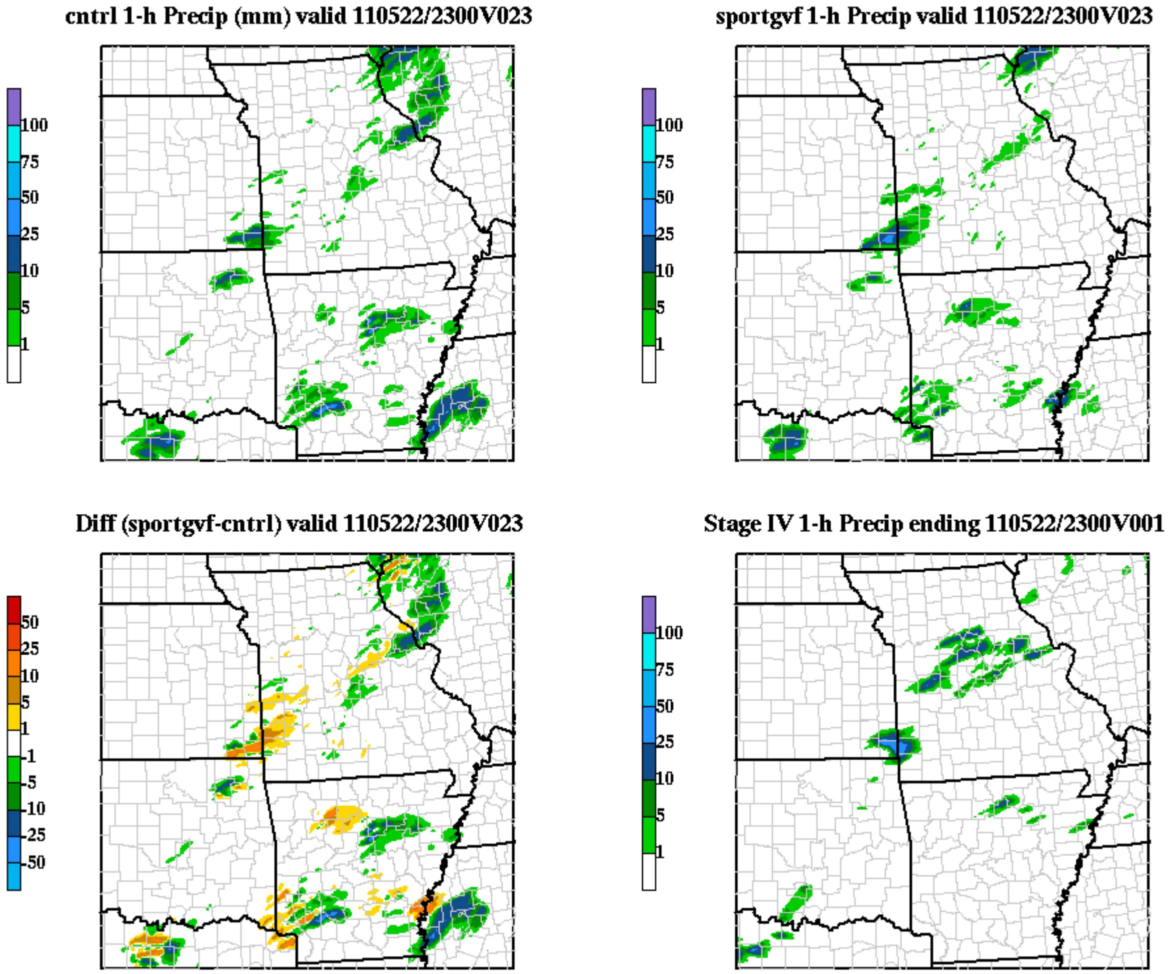

Figure 15. NU-WRF 1-h accumulated precipitation (mm) for the 23-h forecast of the control run (upper-left), sportgvf run (upper-right), difference (bottom-left, sportgvf – control), and stage IV precipitation analysis, valid for the hour ending 2300 UTC 22 May 2011.

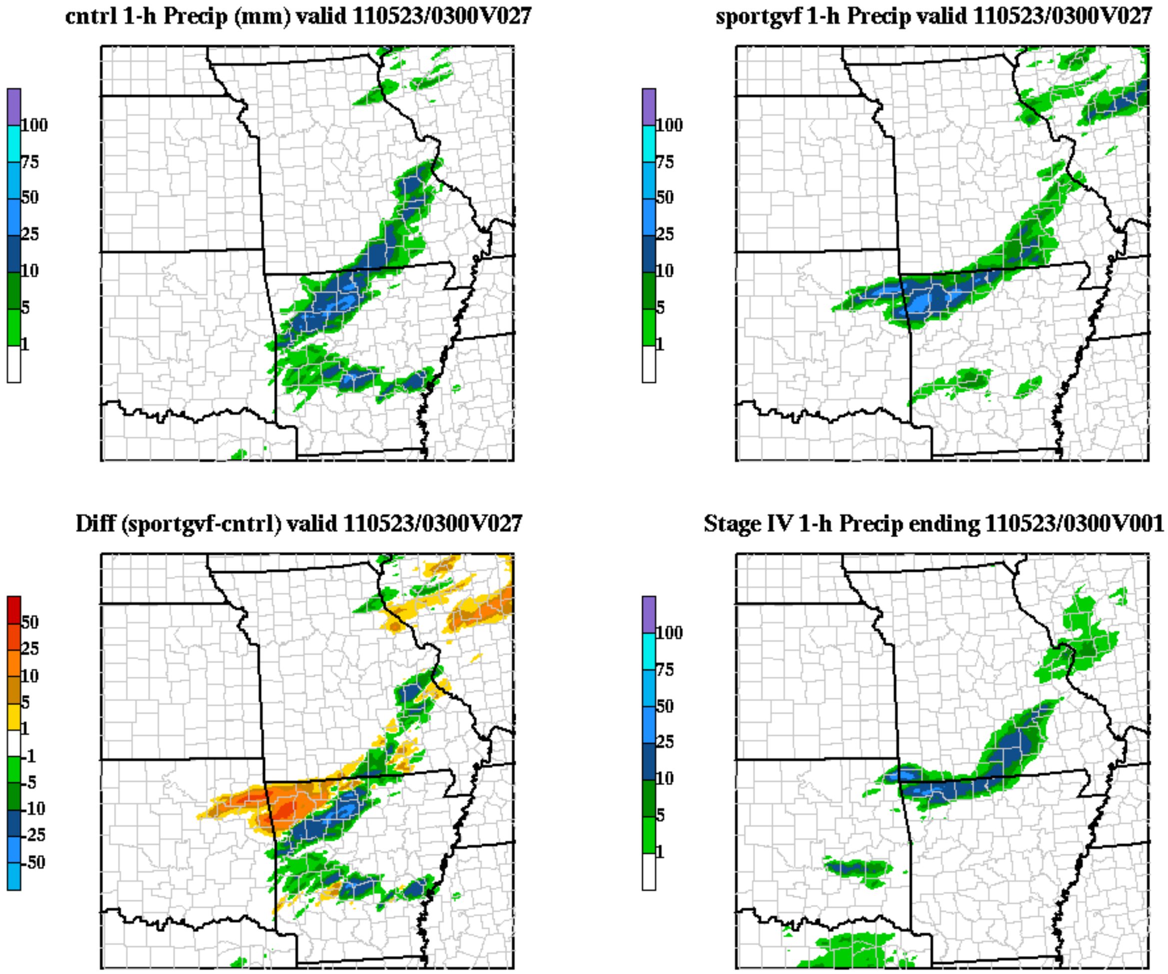

Figure 16. Same as in Figure 15, except for the 27-h forecast for the hour ending 0300 UTC 22 May 2011.